Journal of Solid State Chemistry **167,** 453–458 (2002)
doi:10.1006/jssc.2002.9658

Crystal and Magnetic Structures of $Ba_4Mn_3O_{10}$

V. G. Zubkov,* A. P. Tyutyunnik,* I. F. Berger,* V. I. Voronin,* G. V. Bazuev,* C. A. Moore,† and P. D. Battle†,[1]

*Institute of Solid State Chemistry, Ural Branch of the Russian Academy of Sciences, Ekaterinburg, 620219, Russia; and †Inorganic Chemistry Laboratory, Oxford University, South Parks Road, Oxford OX1 3QR, United Kingdom

Received March 27, 2002; in revised form May 6, 2002; accepted May 13, 2002

A polycrystalline sample of $Ba_4Mn_3O_{10}$ has been prepared and characterized by X-ray diffraction (290 K), neutron diffraction (290, 80, 5 K) and magnetometry ($5 \le T(K) \le 1000$). At 290 K the compound is paramagnetic and isostructural with $Ba_4Ti_2PtO_{10}$. Mn_3O_{12} trimers, built up from MnO_6 octahedra, are linked through common vertices to form corrugated sheets perpendicular to the *y*-axis of the orthorhombic unit cell (Space group *Cmca*, $a = 5.6850(1)$, $b = 13.1284(1)$, $c = 12.7327(1)$ Å); Ba atoms occupy the space between the layers. On cooling, the magnetic susceptibility shows a broad maximum at ~ 130 K, and a sharp transition at 40 K. Neutron diffraction has shown that long-range antiferromagnetic order is present at 5 K but not at 80 K, although magnetometry at 5 K has revealed a remanent magnetization (0.002 μ_B per Mn) which is below the detection limit of the neutron experiment.

INTRODUCTION

Colossal magnetoresistance (CMR) is one of the topics which is currently attracting the attention of solid state chemists (1–3). It has been established that, over a limited temperature range, the resistivity of some mixed-metal oxides containing Mn is reduced by the application of a magnetic field, thus creating the possibility of applications in magnetic switches and data read-out devices. The majority of the Mn oxides under investigation have a pseudo-cubic perovskite structure, which is based on an infinite 3D network of MnO_6 octahedra, linked together by shared vertices. However, CMR has also been observed in the tetragonal $n = 2$ Ruddlesden–Popper phase $Sr_{1.8}La_{1.2}Mn_2O_7$ (4, 5) which can be considered to consist of perovskite-like blocks of MnO_6 octahedra, infinite in the *xy* plane, but having a thickness of only two octahedra parallel to the *z*-axis. It was therefore natural to investigate the properties of other Ruddlesden–Popper phases having the general formula $(A,A')_{n+1}Mn_nO_{3n+1}$, where n is the width (in octahedra) of each perovskite block parallel to *z*. Detailed studies of $n = 3$ $Ca_4Mn_3O_{10}$ (6, 7) have been carried out, but attempts (8, 9) to prepare $Sr_4Mn_3O_{10}$ resulted in the formation of a phase having a crystal structure in which groups of three MnO_6 octahedra share faces to form Mn_3O_{12} groups, these trimers being linked together by shared vertices (Fig. 1); the structural relationship between these different $A_4B_3O_{10}$ phases has been discussed in some detail by Dussarrat et al. (10). Substitution of Sr by Ba (11) showed that this alternative structure was stable when the radius of the alkaline earth cation was increased further, although a composition limit of $Sr_{1.5}Ba_{2.5}Mn_3O_{10}$ was reported. We have now succeeded in extending the stability range to include $Ba_4Mn_3O_{10}$ and we describe below a study of this composition by magnetometry and neutron diffraction. The electronic properties of the trimer-based phases provide an interesting contrast with the Ruddlesden–Popper phases having the same $(A,A')_4Mn_3O_{10}$ stoichiometry, but they are also of interest because trimers, albeit with a different linkage pattern, occur in several hexagonal perovskites, including 9L $BaMnO_3$ (12). The observed properties of these materials are the resultant of intra-trimer and inter-trimer interactions, and the availability of compounds with similar intra-trimer interactions, but different inter-trimer interactions allows us to begin to study the relative importance of the two types of interaction.

EXPERIMENTAL

A polycrystalline sample of $Ba_4Mn_3O_{10}$ was synthesized by the standard methods of solid state chemistry using high-purity barium carbonate (99.9% $BaCO_3$) and manganese dioxide (99.95% MnO_2) as starting materials. A stoichiometric mixture of the reactants was pressed into pellets and annealed in air in an alumina crucible, initially at 950°C for 30 h and then at 1220°C for 24 h. The progress

[1] To whom correspondence should be addressed. Fax: 44-1865-2726-90. E-mail: peter.battle@chem.ox.ac.uk.

0022-4596/02 $35.00

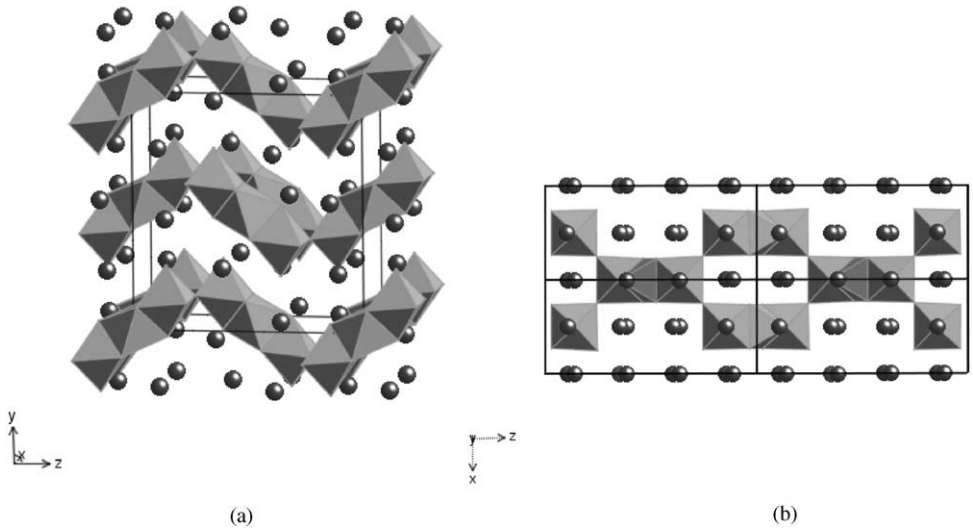

FIG. 1. Crystal structure of $Ba_4Mn_3O_{10}$ (a) viewed along [100] and (b) a single layer viewed down [010]; MnO_6 octahedra are shaded, filled circles represent Ba atoms.

of the reaction was followed by X-ray powder diffraction. The oxygen content of the product was determined by thermogravimetric analysis under flowing hydrogen at 900°C. Initial structural characterization was by X-ray powder diffraction, performed at room temperature using CuKα radiation. Subsequent neutron diffraction studies were carried out at room temperature using the diffractometer 7A at the IWW 2 M reactor (Zarechny) and at 5 and 80 K using the diffractometer D1a at the ILL (Grenoble). Data were collected at the former over the angular range $10 \leq 2\theta(\text{deg}) \leq 100$ with $\Delta 2\theta = 0.1^\circ$ and $\lambda = 1.5220$ Å, and at the latter over the range $10 \leq 2\theta$ (deg) ≤ 160 with $\Delta 2\theta = 0.05^\circ$ and $\lambda = 1.9112$ Å. The sample was contained in a thin-walled aluminum (IBB) or vanadium (ILL) container. All the powder diffraction data were analyzed by the Rietveld method, as implemented in the GSAS program package. The peak shape was fitted using a pseudo-Voigt function, and the background with a Chebyshev polynomial. The magnetic susceptibility of the sample was measured over the temperature range $5 \leq T$ (K) ≤ 1000 in measuring fields $100 \leq H(\text{Oe}) \leq 5000$; data were collected after cooling in the absence of an applied field (ZFC) and after cooling in the measuring field (FC). Measurements at temperatures above 350 K were made using a Faraday balance, those at lower temperatures using a SQUID magnetometer. The field dependence of the magnetisation was measured over the range $-50 \leq H$ (kOe) ≤ 50 after cooling in a field of 50 kOe at 5 K.

RESULTS

Thermogravimetric analysis showed the composition of the reaction product to be $Ba_4Mn_3O_{10.03 \pm 0.03}$. The X-ray powder diffraction pattern could be indexed in an orthorhombic unit cell with $a = 5.6850(1)$, $b = 13.1284(1)$ and $c = 12.7327(1)$ Å in space group *Cmca*. Combined analysis of these data and the corresponding neutron diffraction data by the Rietveld method (13, 14) proceeded smoothly (R_{wp} (X, N) = 3.22, 4.32%) and confirmed that at 290 K $Ba_4Mn_3O_{10}$ is isostructural with $Sr_4Mn_3O_{10}$ and $Ba_4Ti_2PtO_{10}$ (8, 15).The magnetic susceptibility of $Ba_4Mn_3O_{10}$ obeys the Curie–Weiss law in the temperature range $600 \leq T(\text{K}) \leq 1000$, with $\theta = -402$ K and $\mu_{\text{eff}} = 4.06\,\mu_B$ per Mn. The data recorded at lower temperatures (Fig. 2) are more complex. The susceptibility shows a local maximum at 130 K and then rises sharply in a field-dependent manner on cooling below 40 K. Hysteresis is apparent for $H \leq 10$ kOe at 5 K (Fig. 3). The neutron diffraction data collected at 80 K were analyzed in a satisfactory way using the room temperature structure as a starting model; no additional magnetic scattering was observed. The neutron diffraction pattern recorded at 5 K contained additional, low-angle Bragg peaks which had not been observed at room temperature, although they could be indexed without increasing the volume of the unit cell. However, they were not consistent with the presence of a C-centering symmetry operator in the magnetic structure. They were assumed to be magnetic in origin, and the spin arrangement illustrated in Fig. 4, with the spins aligned along x, was found to account ($R_{mag} = 6.5\%$) for their presence (Fig. 5). In deriving this model, in which spin reversal accompanies the C-centering translation associated with the structural space group, it was assumed that all Mn–Mn interactions are inherently antiferromagnetic, and that the intra-trimer interactions are stronger than those between neighboring, vertex-linked trimers. The

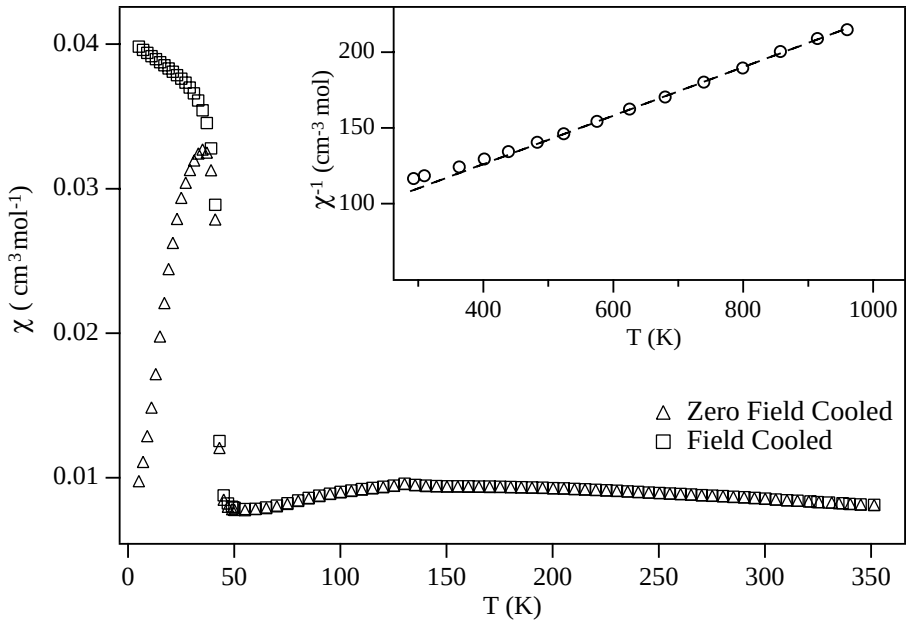

FIG. 2. Molar magnetic susceptibility of $Ba_4Mn_3O_{10}$ as a function of temperature, measured in a field of 1 kOe and (inset) the inverse molar susceptibility in the high-temperature region.

ordered magnetic moments of the crystallographically distinct Mn cations at the centers (Mn1) and ends (Mn2) of the trimers were refined independently and the resulting value for Mn1 (1.98(6) μ_B) is significantly lower than that for Mn2 (2.23(4) μ_B). The results of all our structure refinements are presented in Table 1, and the values of the most significant bond lengths at 290 and 5 K are listed in Table 2. The details of the magnetic model are given in Table 3.

DISCUSSION

$Ba_4Mn_3O_{10}$ is isostructural with $Sr_4Mn_3O_{10}$ and with $Ba_4Ti_2PtO_{10}$, the latter originally (15) being synthesized during a study of ferroelectric $BaTiO_3$. The structure can be considered to consist of corrugated layers perpendicular to the *y*-axis. Short Mn_3O_{12} chains form the basis of the layers, each one of them being formed from three face-sharing MnO_6 octahedra in the sequence Mn2(O1,O2,O3,

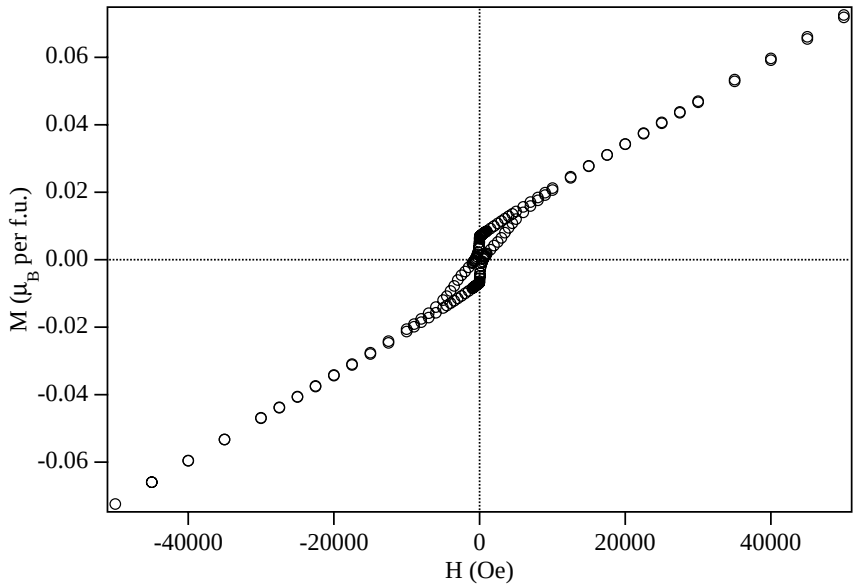

FIG. 3. Magnetization of $Ba_4Mn_3O_{10}$ as a function of applied field at 5 K after cooling in $H = 50$ kOe.

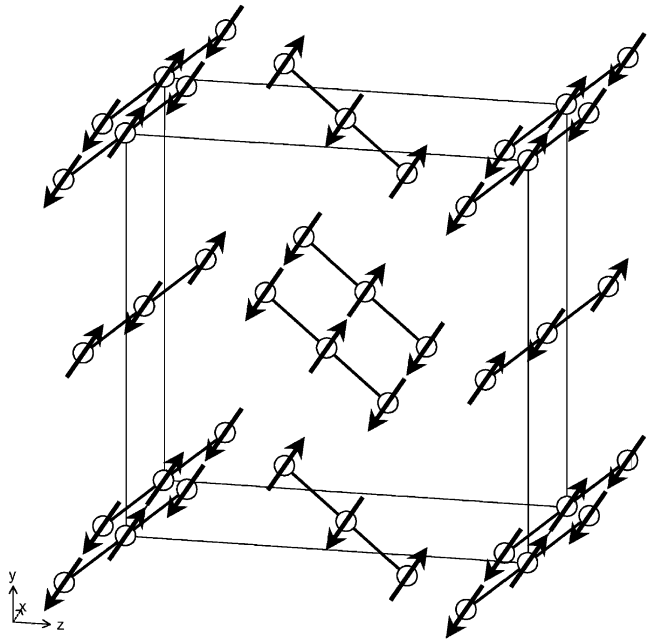

FIG. 4. Magnetic structure of $Ba_4Mn_3O_{10}$; only Mn cations are shown.

O4)–Mn1(O1,O3)–Mn2(O1,O2,O3,O4), as drawn in Fig. 6. If we define the degree of octahedral distortion, σ, as

$$\sigma = \sqrt{\sum_{i=1}^{N} \left| 1 - \frac{R_i}{\sum_{i=1}^{N} R_i/N} \right|^2} \quad \text{where } N = 6,$$

then the degree of distortion of the central octahedra at room temperature ($\sigma = 0.016$) is markedly less than that of the terminal octahedra ($\sigma = 0.118$). The mean Mn1–O and Mn2–O bond lengths, 1.918(4) and 1.936(4) Å, are longer than those found in both $Sr_4Mn_3O_{10}$ and the $n=3$ Ruddlesden–Popper phase $Ca_4Mn_3O_{10}$. They are also significantly longer than those determined in $Sr_{1.5}Ba_{2.5}Mn_3O_{10}$, suggesting that the presence of the large Ba cation allows considerable relaxation in the structure. These short trimeric chains are linked together by shared O4 vertices to form the corrugated *xz* layers, leaving O2 as the only terminal oxide anion. Mn2–O2 is therefore the shortest Mn–O bond in the structure. The Ba1 and Ba2 cations are located in irregular coordination polyhedra, with ten and nine oxide neighbors, respectively. The distortion of the octahedra around Mn1 decreases markedly on cooling to 80 K, although the mean bond length is still relatively long. The Mn–O bond lengths do not change significantly on cooling from 80 to 5 K.

At high temperatures the magnetic susceptibility of $Ba_4Mn_3O_{10}$ obeys the Curie–Weiss law with an effective magnetic moment per Mn cation which is close to the spin-only value and a large, negative Weiss constant which suggests the presence of strong antiferromagnetic interactions. The magnetic behavior of $Ba_4Mn_3O_{10}$ at lower temperatures is very different to that reported for the Sr analogue and $Sr_{1.5}Ba_{2.5}Mn_3O_{10}$; both of these compounds show a susceptibility maximum at $\sim$200 K, which was assumed to indicate the onset of antiferromagnetic ordering. The susceptibility of $Ba_4Mn_3O_{10}$ has a broad maximum at $\sim$130 K, but the absence of magnetic Bragg

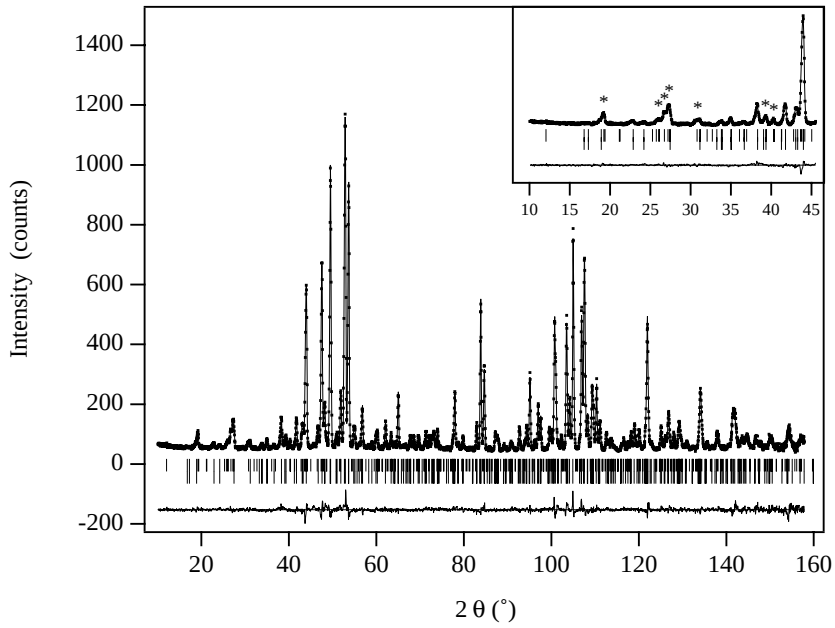

FIG. 5. Observed (.), calculated (-) and difference neutron powder diffraction profiles of $Ba_4Mn_3O_{10}$ at 5 K. Positions of structural (lower) and magnetic (upper) reflections are marked. Strong magnetic reflections at low angle are marked (*) in the inset.

TABLE 1
Structural Parameters of $Ba_4Mn_3O_{10}$ (Space Group *Cmca*) as a Function of Temperature

		290 K	80 K	5 K
a (Å)		5.6850(1)	5.6765(1)	5.67695(8)
b (Å)		13.1284(1)	13.1034(2)	13.1037(2)
c (Å)		12.7327(1)	12.7099(2)	12.7080(2)
V (Å^3)		950.30	945.38(5)	945.34(3)
Ba1, (0,y,z)	y	0.46285(9)	0.4636(2)	0.4630(2)
	z	0.1415(1)	0.1414(2)	0.1414(2)
	U_{iso} (Å^2)	0.0073(4)	0.0018(7)	0.0009(6)
Ba2, (0,y,z)	y	0.2569(1)	0.2572(2)	0.2570(2)
	z	0.3905(1)	0.3894(2)	0.3894(2)
	U_{iso} (Å^2)	0.0100(4)	0.0028(7)	0.0024(7)
Mn1, (0,0,0)	U_{iso} (Å^2)	0.004(1)	0.002(1)	0.001(1)
	μ_x/μ_B	—	—	1.98(6)
Mn2, (0,y,z)	y	0.1257(2)	0.1253(3)	0.1250(3)
	z	0.1530(2)	0.1530(3)	0.1535(3)
	U_{iso} (Å^2)	0.0045(7)	0.0011(9)	0.0018(9)
	μ_x/μ_B	—	—	2.23(4)
O1, (0,y,z)	y	0.0345(3)	0.0339(2)	0.0337(2)
	z	0.8522(4)	0.8535(2)	0.8534(2)
	U_{iso} (Å^2)	0.008(1)	0.0053(7)	0.0031(6)
O2, (0,y,z)	y	0.2643(3)	0.2630(2)	0.2632(2)
	z	0.1453(4)	0.1453(2)	0.1452(2)
	U_{iso} (Å^2)	0.01(1)	0.0042(7)	0.0021(6)
O3, (x,y,z)	x	0.2212(5)	0.2211(3)	0.2221(3)
	y	0.1033(2)	0.1033(1)	0.1034(1)
	z	0.0374(2)	0.0368(1)	0.0366(1)
	U_{iso} (Å^2)	0.0062(6)	0.0016(5)	0.0016(4)
O4 ($\frac{1}{4}$, y, $\frac{1}{4}$)	y	0.1186(3)	0.1186(2)	0.1188(2)
	U_{iso} (Å^2)	0.006(1)	0.0034(7)	0.0042(6)
R_{wp} (%)		3.22/4.32	5.6	5.7
R_I (%)		4.27/2.48 (X-ray/neutron)	3.5	4.3

TABLE 2
Bond Lengths (Å) in $Ba_4Mn_3O_{10}$ at 290 and 5 K

	290 K	5 K
Ba1–O1	2.684(5)	2.694(4)
Ba1–O1′	2.844(2) × 2	2.8396(1) × 2
Ba1–O2	2.607(4)	2.618(4)
Ba1–O3	2.769(3) × 2	2.766(3) × 2
Ba1–O3	2.908(3) × 2	2.892(3) × 2
Ba1–O4	2.848(3) × 2	2.844(3) × 2
Mean Ba1–O	2.803	2.800
Ba2–O1	2.781(4)	2.780(4)
Ba2–O2	2.881(1) × 2	2.7834(5) × 2
Ba2–O3	2.907(3) × 2	2.905(3) × 2
Ba2–O3	2.726(3) × 2	2.725(3) × 2
Ba2–O4	2.919(3) × 2	2.904 (3) × 2
Mean Ba2–O	2.849	2.824
Mn1–O1	1.936(5) × 2	1.915(3) × 2
Mn1–O3	1.909(2) × 4	1.908(2) × 4
Mean Mn1–O	1.918	1.910
Mn2–O1	2.106(5)	2.081(5)
Mn2–O2	1.822(5)	1.815(5)
Mn2–O3	1.958(3) × 2	1.970(3) × 2
Mn2–O4	1.886(2) × 2	1.877(2) × 2
Mean Mn2–O	1.936	1.932
Mn1–Mn2	2.554(3)	2.547(4)

scattering in the neutron diffraction pattern recorded at 80 K proves that this does not correspond to a Néel temperature. It is likely that the maximum is caused by short-range spin pairing within the xz layers. We believe that the transition to a state with true, long-range magnetic order occurs at 40 K, at which temperature a more obvious anomaly is observed in the susceptibility. The sharp but limited rise shown by the susceptibility, together with the development of hysteresis below the transition, suggests that the low-temperature phase is a weak ferromagnet, a remanent magnetization of $\sim 0.002\,\mu_B$ per Mn being observed at 5 K. However, only the dominant antiferromagnetic component of the magnetic structure could be detected by neutron diffraction. The details of the antiferromagnetic structure were deduced by making a simple assumption about the relative strengths of the competing superexchange interactions. The refined value of the atomic magnetic moment of Mn2 is typical of those observed previously (6) for Mn^{4+} oxides, the reduction from the spin-only value ($3\,\mu_B$) being due to a combination of covalency and zero-point effects. However, the value of $1.98(6)\,\mu_B$ observed for Mn1 is somewhat lower. We attribute the difference in the ordered magnetic moments of Mn1 and Mn2 to the different bonding environments experienced by cations in octahedra with different linkage patterns; the covalent interactions are likely to be greater in an octahedron which shares two faces with neighboring polyhedra.

The onset of long-range magnetic order at a temperature well below that of a susceptibility maximum has been reported in a number of Mn oxides with hexagonal perovskite-like structures. It has been shown (16) that the Néel temperature of 2 H $BaMnO_3$ is 59 K, although the

TABLE 3
Magnetic Structure of $Ba_4Mn_3O_{10}$

Atom	Site	Ordered moment (μ_B)
Mn1	0, 0, 0	1.98(6)
Mn1	0, $\frac{1}{2}$, $\frac{1}{2}$	1.98(6)
Mn2	0, y, z	−2.23(4)
Mn2	0, $\frac{1}{2}-y$, $\frac{1}{2}+z$	−2.23(4)
Mn2	0, $\frac{1}{2}+y$, $\frac{1}{2}-z$	−2.23(4)
Mn2	0, $-y$, $-z$	−2.23(4)

Note. Equal and opposite moments at $(\frac{1}{2}, \frac{1}{2}, 0) + y = 0.1250(3)$, $z = 0.1535(3)$.

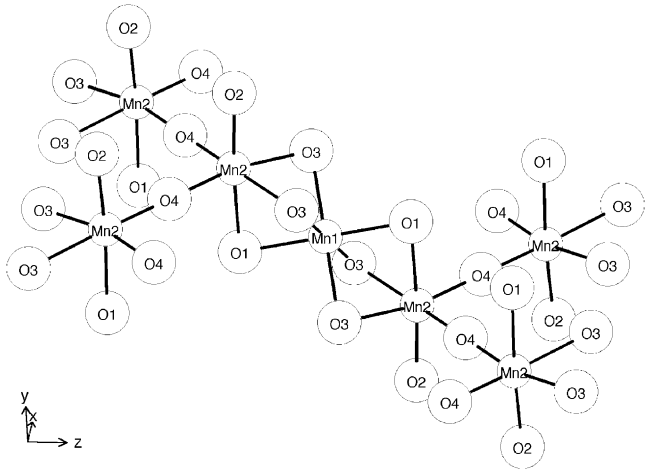

FIG. 6. Mn_3O_{12} unit in $Ba_4Mn_3O_{10}$ showing the links to four neighboring units through O4 vertex-sharing.

susceptibility has a local maximum at $\sim$150 K. Similarly, the susceptibility of $Ba_6ZnMn_4O_{15}$ has a maximum at 40 K (17), but the Néel temperature is 6 K (18). However, whereas the behavior of $Ba_4Mn_3O_{10}$ derives from the 2D nature of the structure, these two compounds, built up from chains of face-sharing MnO_6 octahedra, have strong 1D characteristics, and the measured value of the ordered magnetic moment of Mn^{4+} ($1.31(5)\,\mu_B$ in $BaMnO_3$) is reduced by the effects of frustration. The pattern of face- and vertex-sharing octahedra found in $Ba_4Mn_3O_{10}$ eliminates frustration, and a larger moment is observed. However, the introduction of vertex-sharing linkages between some of the MnO_6 octahedra reduces the concentration of short (2.55 Å) Mn–Mn interactions to the extent that, despite the absence of frustration and the increase in structural dimensionality, the Néel temperatures of 2H $BaMnO_3$ and $Ba_4Mn_3O_{10}$ are very similar. Only limited magnetic data are available (12) on 9R $BaMnO_3$, but a susceptibility maximum is observed at $\sim$300 K, showing that the magnetic interactions are stronger when the Mn_3O_{12} trimers link to form a 3D network, rather than a layered structure. $Ba_4Ru_3O_{10}$, containing a second-row magnetic cation, is isostructural (19, 20) with $Ba_4Mn_3O_{10}$ and shows a broad susceptibility maximum at $\sim$150 K with a subsequent upturn on cooling below $\sim$50 K. Although hysteresis measurements and neutron diffraction data are not available for the Ru phase, it appears that these two compounds may have similar magnetic properties; the Ru–Ru distance within the trimers of $Ba_4Ru_3O_{10}$ is 2.56 Å, essentially the same as the comparable distance in the Mn analogue. We note that the temperature offset between the Néel point and the susceptibility maximum in these systems necessitates the use of neutron diffraction in any complete determination of their magnetic properties.

ACKNOWLEDGMENTS

We acknowledge experimental assistance from Thomas Hansen at ILL Grenoble, and funding from EPSRC. Magnetic susceptibility measurements above 350 K were performed by D. G. Kellerman.

REFERENCES

1. C. N. R. Rao and A. K. Cheetham, *Adv. Mater.* **9,** 1009 (1997).
2. C. N. R. Rao, A. K. Cheetham, and R. Mahesh, *Chem. Mater.* **8,** 2421 (1996).
3. A. P. Ramirez, *J. Phys.: Condens. Matter* **9,** 8171 (1997).
4. Y. Moritomo, A. Asamitsu, H. Kuwahara, and Y. Tokura, *Nature* **380,** 141 (1996).
5. P. D. Battle and M. J. Rosseinsky, *Curr. Opin. Solid State Mater. Sci.* **4,** 163 (1999).
6. P. D. Battle, M. A. Green, J. Lago, J. E. Millburn, M. J. Rosseinsky, and J. F. Vente, *Chem. Mater.* **10,** 658 (1998).
7. J. Lago, P. D. Battle, and M. J. Rosseinsky, *J. Phys.: Condens. Matter* **12,** 2505 (2000).
8. J. Fabry, J. Hybler, Z. Jirak, K. Jurek, K. Maly, M. Nevriva, and V. Petricek, *J. Solid State Chem.* **73,** 520 (1988).
9. H. J. Rossell, P. Goodman, S. Bulcock, R. H. March, S. J. Kennedy, T. J. White, F. J. Lincoln, and K. S. Murray, *Aust. J. Chem.* **49,** 205 (1996).
10. C. Dussarrat, F. Grasset, and J. Darriet, *Eur. J. Solid State Chem.* **32,** 557 (1995).
11. N. Floros, M. Hervieu, G. v. Tendeloo, C. Michel, A. Maignan, and B. Raveau, *Solid State Sciences* **2,** 1 (2000).
12. B. L. Chamberland, A. W. Sleight, and J. F. Weiher, *J. Solid State Chem.* **1,** 506 (1970).
13. H. M. Rietveld, *J. Appl. Crystallogr.* **2,** 65 (1969).
14. A. C. Larson and R. B. von-Dreele, "General Structure Analysis System (GSAS)." Report LAUR 86-748, *Los Alamos National Laboratories*, 1990.
15. H. Blattner, H. Gränicher, W. Känzig, and W. Merz, *Helv. Phys. Acta* **21,** 341 (1948).
16. E. J. Cussen and P. D. Battle, *Chem. Mater.* **12,** 831 (2000).
17. E. J. Cussen, J. F. Vente, and P. D. Battle, *J. Amer. Chem. Soc.* **121,** 3958 (1999).
18. P. D. Battle and E. J. Cussen, *Mater. Res. Soc. Symp. Proc.* **658,** GG2.4.1 (2001).
19. A. H. Carim, P. Dera, L. W. Finger, B. Mysen, C. T. Prewitt, and D. G. Schlom, *J. Solid State Chem.* **149,** 137 (2000).
20. C. Dussarrat, F. Grasset, R. Bontchev, and J. Darriet, *J. Alloys Compd.* **233,** 15 (1996).